Extracellular Space Volume Measured by Two-Color Pulsed Dye Infusion with Microfiberoptic Fluorescence Photodetection

Mazin Magzoub,[†] Hua Zhang,[†] James A. Dix,[‡] and A. S. Verkman[†*]
[†]Departments of Medicine and Physiology, University of California, San Francisco, California; and [‡]Department of Chemistry, State University of New York at Binghamton, Binghamton, New York

ABSTRACT The extracellular space (ECS) is the aqueous matrix surrounding cells in solid tissues. The only method to measure ECS volume fraction (α) in vivo has been tetramethylammonium iontophoresis, a technically challenging method developed more than 25 years ago. We report a simple, quantitative method to measure α by microfiberoptic fluorescence detection of a self-quenched green dye, calcein, and a reference red dye, sulforhodamine 101, after pulsed iontophoretic infusion. The idea is that the maximum increase in calcein fluorescence after iontophoresis is proportional to the aqueous volume into which the dye is deposited. We validated the method theoretically, and experimentally, using cell-embedded gels with specified α and ECS viscosity. Measurements in living mice gave α of 0.20 $\pm$ 0.01 in brain, 0.13 $\pm$ 0.02 in kidney and 0.074 $\pm$ 0.01 in skeletal muscle. The technical simplicity of the "pulsed-infusion microfiberoptic photodetection" method developed here should allow elucidation of the relatively understudied biological roles of the ECS.

INTRODUCTION

The extracellular space (ECS) is the space between immobile cells in solid tissues, consisting of a tissue-specific, jelly-like, extracellular matrix. The ECS has been studied most extensively in the central nervous system, where it represents ~20% of brain parenchymal volume under normal conditions and can change in response to altered serum osmolality and neuronal excitation, and under pathological conditions such as anoxia, brain tumors and edema (1,2). The ECS in the brain is important for nonsynaptic intercellular communication, delivery of drugs to cells, elimination of neurotransmitters, and extracellular K^+ and glutamate buffering (3,4). Limited information, primarily from dye partitioning, is available about ECS volume in other solid organs such as kidney and skeletal muscle (5). Extracellular space size and diffusion is also of importance in tumors for delivery of anti-cancer therapies (6,7).

The key physical parameters describing the ECS include its volume fraction, α, and its tortuosity, λ, the latter being related to hindrance to solute diffusion in the ECS by ECS geometry and extracellular matrix viscosity. Although various single- and multiphoton methods have been developed and applied to measure diffusion of probe molecules in tissues in vivo (8–11), to date the only approach to measure α in vivo has been the tetramethylammonium (TMA^+) method, which has been applied exclusively to brain tissue. The TMA^+ method involves pulsed iontophoretic delivery of TMA^+, and microelectrode detection of [TMA^+] as it is deposited into and diffuses away from a detection site near the delivery site (12). Determination of α is based on changes in [TMA^+] after iontophoresis over tens of seconds, which provide a measure of the extracellular aqueous volume of TMA^+ dilution. However, the TMA^+ method is technically challenging and requires complex analysis (see Discussion section), such that it has been used by only two laboratories in the 25 years after its original description.

We report a technically simple optical method to measure α. The principle of our ''Pulsed-Infusion Microfiberoptic Photodetection'' (PIMP) method is the simultaneous microfiberoptic detection of the fluorescence of two dyes (calcein, at self-quenching concentration, and sulforhodamine 101 (SR), which does not undergo self-quenching) after pulsed delivery by iontophoresis (Fig. 1 *A*). As explained in the Results section and modeled in the Appendix, the maximum increase in calcein fluorescence after iontophoresis is linearly related to ECS volume fraction, α, whereas the SR fluorescence increase is independent of α. The kinetics of SR fluorescence decay provides a direct measure of its diffusion coefficient, D. We constructed the instrumentation for α and D determination by PIMP, validated the method and analysis procedures using cell-embedded gels, and measured α in several solid organs.

EXPERIMENTAL METHODS

Instrumentation

PIMP measurements were done by pulsed infusion of fluorescent dyes through a micropipette positioned at a specified distance (typically 20 μm) from the tip of a microfiberoptic (Fig. 1 *B*). The apparatus consists of an iontophoretic dye infusion system, a two-color microfiberoptic fluorescence detection system, and hardware for precise positioning of the injection micropipette and the microfiberoptic tip deep in solid, opaque tissues.

A single-channel iontophoresis current generator (Dagan, Minneapolis, MN) was used to deliver an aqueous solution containing calcein (100 mM) and SR (2 mM) (both from Sigma-Aldrich, St. Louis, MO, fluorescence

Submitted November 14, 2008, and accepted for publication December 8, 2008.

*Correspondence: Alan.Verkman@ucsf.edu; http://www.ucsf.edu/verklab

Editor: Gerard Marriott.

0006-3495/09/03/2382/9 $2.00

doi: 10.1016/j.bpj.2008.12.3916

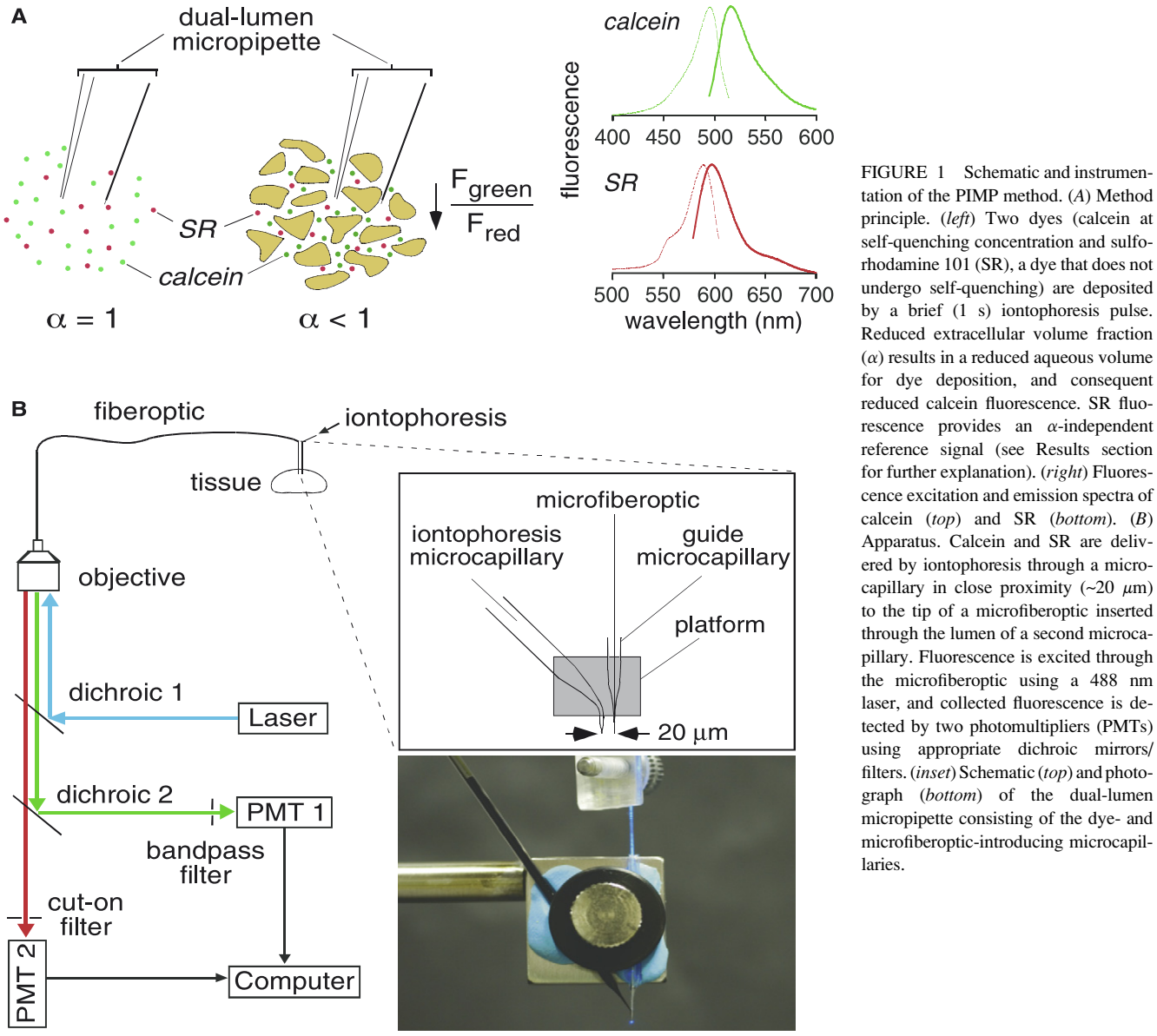

FIGURE 1 Schematic and instrumentation of the PIMP method. (*A*) Method principle. (*left*) Two dyes (calcein at self-quenching concentration and sulforhodamine 101 (SR), a dye that does not undergo self-quenching) are deposited by a brief (1 s) iontophoresis pulse. Reduced extracellular volume fraction (α) results in a reduced aqueous volume for dye deposition, and consequent reduced calcein fluorescence. SR fluorescence provides an α-independent reference signal (see Results section for further explanation). (*right*) Fluorescence excitation and emission spectra of calcein (*top*) and SR (*bottom*). (*B*) Apparatus. Calcein and SR are delivered by iontophoresis through a microcapillary in close proximity (~20 μm) to the tip of a microfiberoptic inserted through the lumen of a second microcapillary. Fluorescence is excited through the microfiberoptic using a 488 nm laser, and collected fluorescence is detected by two photomultipliers (PMTs) using appropriate dichroic mirrors/filters. (*inset*) Schematic (*top*) and photograph (*bottom*) of the dual-lumen micropipette consisting of the dye- and microfiberoptic-introducing microcapillaries.

spectra shown in Fig. 1 *A*, *right*) through a glass micropipette. Generally, the iontophoresis current was set to 2 μA for a duration of 1 s.

Dye fluorescence was detected using an epifluorescence microscope (Diaphot; Nikon, Melville, NY) in which a laser beam (20 mW at 488 nm; Coherent, Santa Clara, CA) was focused onto the back of a 62.5 μm core-diameter multimode fiberoptic (ThorLaboratories, Newton, NJ) with ferule connector using a 20× objective lens (numerical aperture, 0.25; Carl Zeiss, Maple Grove, MN). The distal end of the fiber was stripped and chemically etched as described (10) to create a micron-sized tip, which was visualized using a Leica DM 4000B microscope (Leica Microsystems, Bannockburn, IL). The shaft near the fiber tip was coated with a thin layer of aluminum (~10 nm) by rotary sputtering (Evaporated Coatings, Willow Grove, PA) to minimize light loss and prevent detection of fluorescence along the tapered fiber shaft. The fiberoptic tip illuminated a small approximately cone-shaped volume of tissue (10).

Calcein and SR fluorescence were recorded continuously. Fluorescence collected by the microfiberoptic and objective lens was filtered (490 nm dichroic mirror, 510 nm long-pass filter; Chroma Technology, Rockingham, VT), split at 90° by a second dichroic mirror (580 nm; Chroma), and detected by two photomultipiers through appropriate filters (calcein, 540 ± 25 nm band-pass filter; SR, 610 nm long-pass filter; Chroma). Amplified signals were digitized and recorded at 5–20 Hz.

Dual-lumen micropipette

To achieve efficient and standardized dye delivery deep in tissues, a dual-lumen micropipette was constructed using borosilicate glass microcapillaries. For dye introduction, a single barrel microcapillary without filament (inner diameter 0.75 mm; FHC, Bowdoin, ME) was pulled on a horizontal pipette puller (Sutter Instrument, Novato, CA) to a tip diameter of ~1 μm. A bend of 60 degrees was created ~3 mm from the tip (Fig. 1 *B*, *inset*) using a microforge (Narishige, Los Angeles, CA). A second pulled microcapillary was created as a guide for the optical fiber. The guide consisted of a 4 mm long glass microcapillary with tip diameter ~20 μm to allow the microfiber to pass freely through the lumen. The dye-introducing and fiber-guide microcapillaries were immobilized on a rectangular platform of a custom-built aluminum plate, with the tip of the guide microcapillary positioned 3 mm proximal to the tip of the dye-introducing microcapillary (Fig. 1 *B*, *inset*). The two microcapillaries were aligned under a microscope to be parallel with an ~20 μm separation between the microfiberoptic and

microinjection tips. The dual-lumen micropipette and optical fiber were secured separately using micromanipulators (World Precision Instruments, Sarasota, FL), allowing insertion to specific depths in tissue with accuracy of ~2 μm. To prevent blockage, a small positive pressure is applied during insertion into tissues until the dual-lumen micropipette is close to the measurement site. Also, the fiberoptic tip was rinsed between measurements.

In vitro measurements

For preparation of cell-embedded agarose gels, SP 2/0 Ag14 cells (ATCC No. CRL-1581) were cultured in Dulbecco's modified Eagle's medium containing 4.5 g/L glucose (DME-H21) supplemented with L-glutamine (0.58 g/L), penicillin (100 U/ml), streptomycin (0.1 mg/ml) and 10% fetal bovine serum. These cells were chosen for their rapid growth in suspension medium and uniform spherical shape and size. After centrifugation, the cell pellet was suspended in culture medium containing 0.3% agarose, which was allowed to solidify. A sample taken before gelation was used for the determination of cell density using a hemocytometer. ECS volume fraction, α, was computed from cell density and average cell volume (diameter = 10.4 $\pm$ 0.4 μm, as determined by imaging). In some experiments, ECS viscosity was increased by adding 10 or 15% wt/wt Ficoll-70 (η/η_0 = 3 or 5, respectively), or sample turbidity was increased by addition of nonfat dry milk (8% wt/vol).

Determination of α and D

As described in the Appendix, α is determined from the maximum increase in calcein fluorescence, ΔF_{cal}, after iontophoresis,

$$\alpha = \Delta F_{cal}^{test} / \Delta F_{cal}^{ref}, \quad (1)$$

where the test and ref superscripts refer to test and reference ($\alpha = 1$ gel) samples, respectively. Relative SR diffusion in reference versus test samples, D_o/D, is determined directly from half-times ($t_{1/2}$) for decay of SR fluorescence to 50% of its peak value,

$$D_0/D = t_{1/2}^{test} / t_{1/2}^{ref}. \quad (2)$$

In vivo measurements

Measurements were done on male weight-matched (25–30 g) mice in a CD1 genetic background that were maintained in air-filtered cages and fed normal mouse chow in the University of California, San Francisco Animal Care facility. Mice were anesthetized with 2,2,2-tribromoethanol (avertin; Sigma) (i.p. 125 mg/kg) and immobilized in a stereotactic frame (MyNeuroLab, St. Louis, MO). Additional avertin was given as needed. During experiments core temperature was monitored using a rectal probe and maintained at 37–38°C using a heating lamp.

Brain measurements were made in the parietal cortex at a depth of 400 μm, with surgery done as described (13). A midline incision was made above the sagittal suture and a craniotomy was created using a high-speed microdrill (MyNeuroLab) under an operating microscope. The dura was carefully removed and the cerebral surface was irrigated continuously with artificial cerebrospinal fluid (aCSF) (in mM: NaCl, 145; KCl, 4; $MgCl_2$, 1; $CaCl_2$, 2.5; KH_2PO_4, 1; glucose, 10; pH 7.4) at 37–38°C. For measurements in the kidney, the right kidney was exposed by a ventral laparotomy. After a horizontal incision, the skin, abdominal muscles and intestines were retracted and the kidney was dissected from the retroperitoneum and stabilized. Under an operating microscope, the capsule was incised and the cortex of the kidney was exposed. The microfiberoptic was inserted through the dual-lumen device to a depth of 400 μm. Measurements in skeletal muscle were made in the gluteus maximus muscle. An axial incision was made above the hip joint exposing the muscle surface. The fascia was carefully elevated and incised to access the underlying fibers. The microfiberoptic was inserted through the thin layer of connective tissue into muscle tissue to a depth of 400 μm.

RESULTS

Method principle and instrumentation

Fig. 1 *A* illustrates the principle of the PIMP method for determination of ECS volume fraction (α) and tortuosity (λ). Tortuosity is defined by the relation $\lambda = \sqrt{(D_o/D)}$, where D_o and D are the diffusion coefficients in water and ECS, respectively. A brief (1 s) iontophoresis pulse causes the local deposition of self-quenched calcein and SR molecules over a distance greater than the separation between the delivery and measurement sites. After deposition, the dyes diffuse away from the deposition volume over time. The time course of calcein fluorescence is related to both calcein diffusion and self-quenching. As SR is not subject to self-quenching, the SR fluorescence time course depends only on SR diffusion. Experimentally, the fluorescence time courses after dye infusion in a ''test'' sample (such as brain tissue, $\alpha < 1$) is compared to a ''reference'' sample (0.3% agarose gel, $\alpha = 1$). Provided that the calcein concentration, [calcein], deposited at the detection site is on the downward, self-quenching portion of the fluorescence versus [calcein] relation (i.e., [calcein] >3 mM, Fig. 2 *C*), then as calcein diffuses away, its fluorescence at the detection site will initially increase (due to loss of self-quenching) to a maximum value when [calcein] ~ 3 mM. This maximum increase in calcein fluorescence is proportional to α, since calcein molecules in a detected volume element are distributed in volume fraction α. Thus, the ratio of the maximum increase in calcein fluorescence in test versus reference samples is simply equal to α. The ratio of half-times ($t_{1/2}$) for decay of SR fluorescence in the test versus reference samples is equal to D_o/D.

As diagrammed in Fig. 1 *B*, measurements are done deep in solid tissues by insertion of a microfiberoptic with micron-size tip through the lumen of a microcapillary (Fig. 1 *B*, *inset*). Calcein and SR are delivered by iontophoresis through a second lumen separated from the tip of the microfiberoptic by ~20 μm. The dye concentrations and separation distance were chosen to ensure strong fluorescence signals after 1 s iontophoresis, and that the [calcein] deposited at the detection site is on the downward portion of the fluorescence versus [calcein] relation. With single wavelength excitation, calcein and SR fluorescence collected through the microfiberoptic are detected simultaneously using a dichroic mirror, filters, and two photomultipliers.

Experimental validation

We used cell-embedded gels to simulate solid tissues having cellular and extracellular compartments, in which specified densities of live spherical cells were suspended in 0.3% agarose gels. ECS volume fraction α was determined from cell density and size, and ECS viscosity from the concentration of added Ficoll-70. Measurements were done for α of 1.0 (agarose gel not containing cells), 0.42, 0.21 and 0.12. Light micrographs of the cell-embedded gels are shown in Fig. 2 *A*.

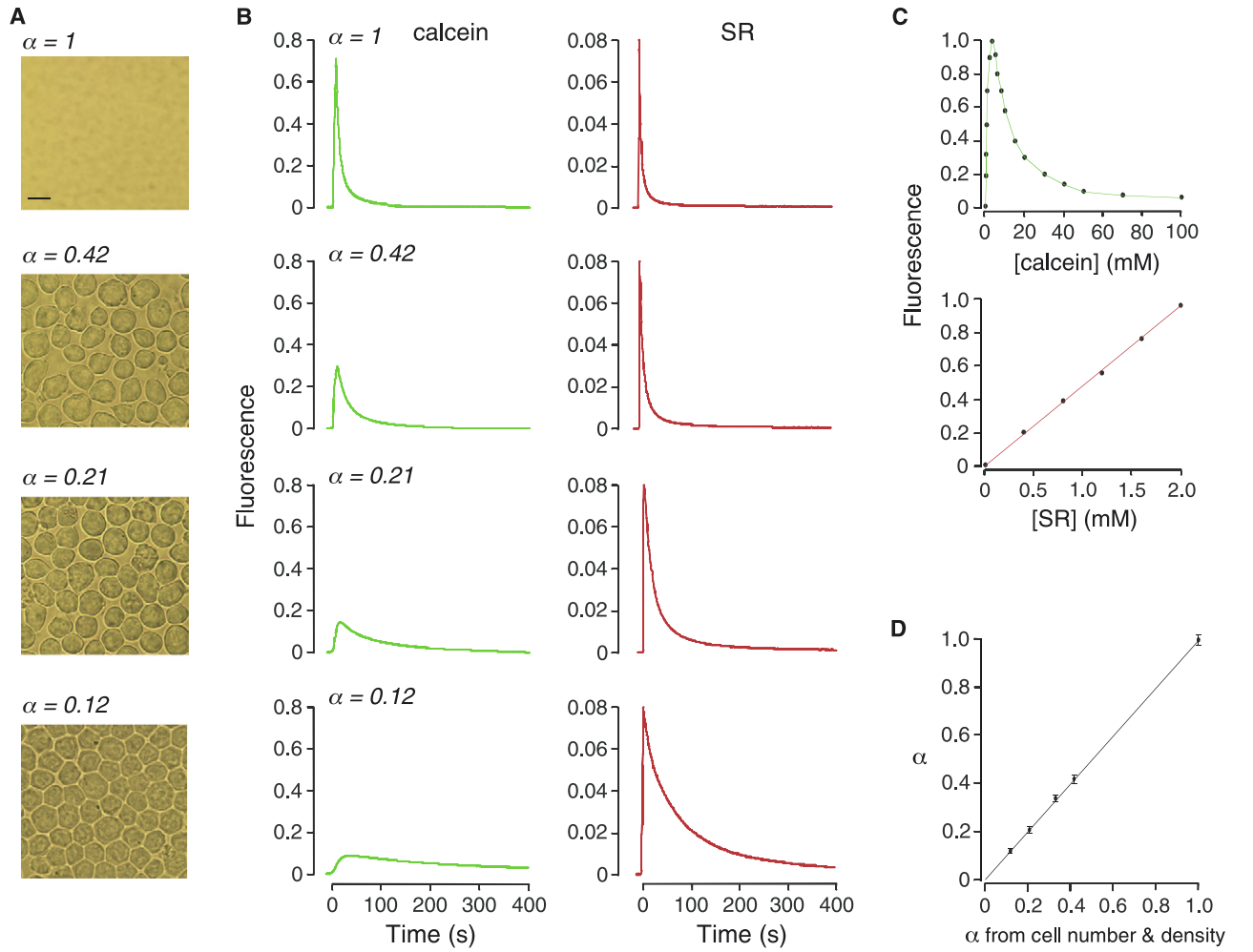

FIGURE 2 Extracellular space volume measurements in cell-embedded gels. (*A*) Brightfield micrographs of cell-embedded agarose gels containing different densities of SP2/0 cells in 0.3% agarose, giving α of 1 (gel not containing cells), 0.42, 0.21 and 0.12. (*B*) Time course of calcein (*left panels*) and SR (*right panels*) fluorescence after pulsed iontophoretic dye delivery into the gels. (*C*) Dependence of calcein (*top*) and SR (*bottom*) fluorescence, in agarose gels (at physiological pH and osmolarity), on their concentration. (*D*) Summary of measured α from experiments as in *B* versus specified α (from cell volume and density) (SE n = 4).

Fig. 2 *B* shows the time courses of calcein and SR fluorescence measured for each of the gels. The fluorescent dyes were introduced by a 1 s iontophoresis pulse. The resultant detected fluorescence curves had excellent signal/noise ratios of >100:1, and were highly reproducible. With decreasing α, the amplitudes of the calcein fluorescence curves were reduced. As discussed above, the amplitude of the maximum increase in calcein fluorescence, normalized to the amplitude of the calcein curve in the reference ($\alpha = 1$) gel, is equal to α. A strict requirement of the PIMP method is that [calcein] at the detection site just after iontophoresis is >3 mM (where calcein fluorescence is maximum) as measured in gels (at physiological pH and osmolarity) containing specific [calcein] (Fig. 2 *C*, *top*). This requirement was verified in each set of experiments from measured SR fluorescence (as in Fig. 2 *C*, *bottom*), knowing [calcein] and [SR] in the infusion pipette.

In contrast to calcein fluorescence, the amplitudes of the SR fluorescence curves were not affected by difference in α (Fig. 2 *B*, *right*), as predicted when iontophoretic dye delivery is much faster than diffusion. However, the kinetics of fluorescence decay was slowed with increasing cell density because of reduced SR diffusion in the more crowded, tortuous ECS. Another key feature of the fluorescence data is a greater delay in reaching maximum calcein fluorescence with reduced α, which is a consequence of greater [calcein] (and self-quenching) just after iontophoresis. Fig. 2 *D* summarizes α from experiments as in Fig. 2 *B*, showing excellent agreement between the experimentally measured α and that determined from cell size and density.

A series of additional measurements were done to validate the determination of α from fluorescence data. First, we varied *D* keeping α fixed by the addition of a membrane-impermeant viscous macromolecule, Ficoll-70, to the agarose gels in which the cells were suspended. As shown in Fig. 3 *A*, the addition of Ficoll-70 did not affect the initial increase in calcein or SR fluorescence in either the $\alpha = 1$

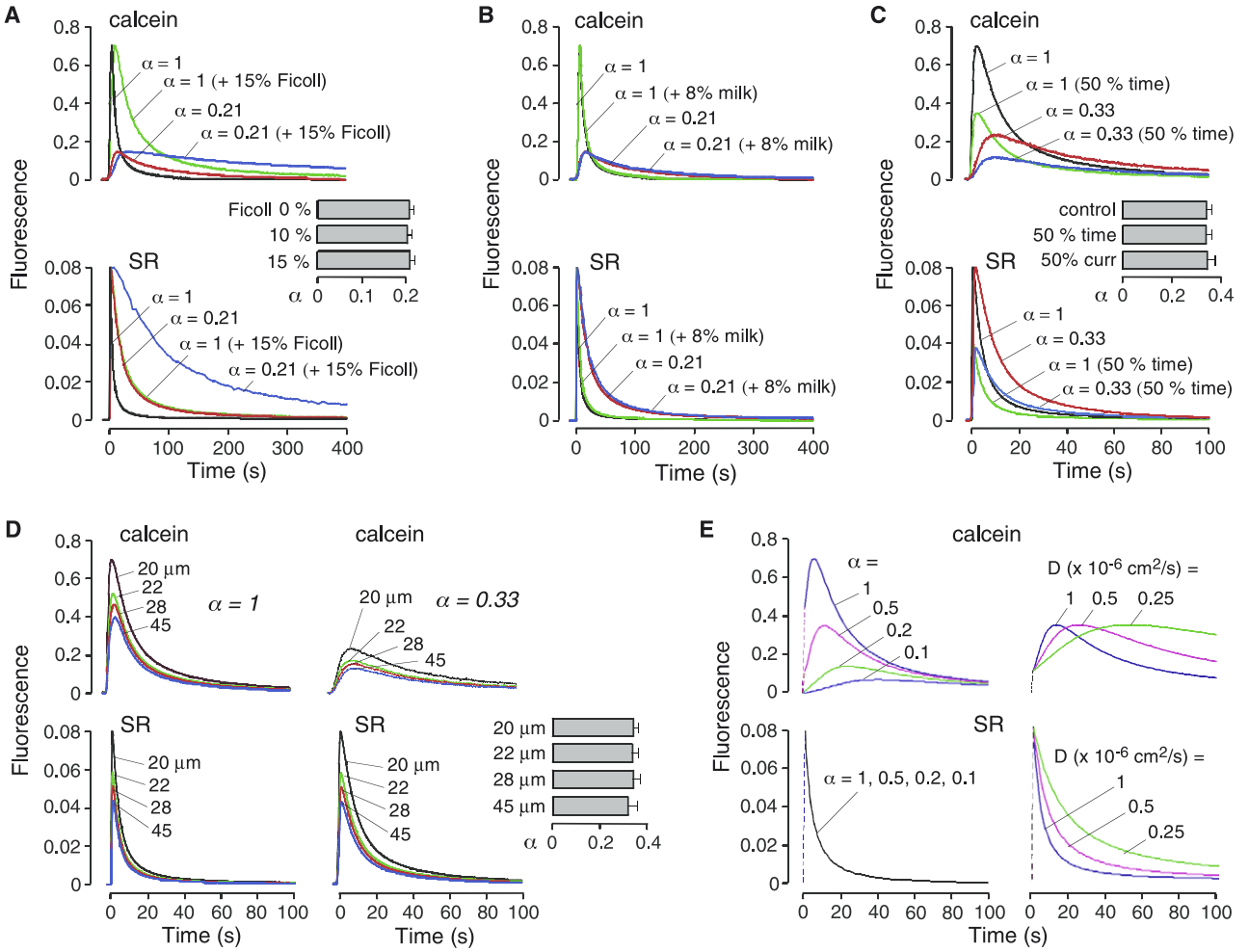

FIGURE 3 Experimental and theoretical validation of α determination by the PIMP method. (*A*) Calcein (*top*) and SR (*bottom*) fluorescence data on cell-embedded agarose gels with $\alpha = 0.21$, compared with reference sample (agarose gel without cells, $\alpha = 1$), in which ECS viscosity was increased by addition of Ficoll-70 (10 or 15% wt/wt). (*inset*) Summary of α values (SE, n = 3) (*B*) Measurements as in *A* in which sample turbidity was increased by addition of 8% wt/wt powdered nonfat milk. (*C*) Data on reference and cell-embedded gels with $\alpha = 0.33$ as in *A* and with 50% reduction in iontophoresis time or current. (*D*) Data on reference and cell-embedded gels with $\alpha = 0.33$ at different separations between iontophoresis and microfiberoptic detection sites. (*E*) Theoretical curves of calcein and SR fluorescence as a function of α and D, computed as described in the Appendix. (*left*) Calcein (*top*) and SR (*bottom*) fluorescence computed for different α (1, 0.5, 0.2 and 0.1) at constant $D = 1 \times 10^{-6}$ cm^2/s. The initial dashed lines represent the increase in fluorescence intensity from iontophoresis. (*right*) Calcein (*top*) and SR (*bottom*) fluorescence computed for different D (1.0, 0.5 and 0.25 $\times 10^{-6}$ cm^2/s) at constant $\alpha = 0.5$.

(cell-free) gel or the $\alpha = 0.21$ (cell-embedded) gel, though the fluorescence decay was slowed. The half-times for the SR fluorescence decay were increased by three- and fivefold for 10 (data not shown) and 15% Ficoll-70 (compared to 0 Ficoll-70), respectively, in agreement with the increases in solution viscosities of three- and fivefold (14). Computed α values were independent of D, as expected (Fig. 3 *A*, *inset*).

Next, we examined the possible effects of tissue light scattering, which could affect the precise illumination and detection volumes, secondarily affecting signal amplitudes and curve shapes. Fig. 3 *B* shows that the addition of 8% nonfat milk to gels, which produces greater light scattering than brain tissue (10,15), had no demonstrable effect on calcein or SR fluorescence curves.

The cell-embedded gel system was also used to investigate the sensitivity of α to iontophoresis conditions (time and current) and the distance between iontophoresis and microfiberoptic detection sites. Fig. 3 *C* shows calcein and SR curves obtained in cell-free and cell-embedded gels under standard conditions (1 s iontophoresis time and 2 μA current) and with 50% reduced time or current, which produced the expected reductions in signal amplitude. Computed α did not depend on iontophoresis time or current (Fig. 3 *C*, *inset*). Fig. 3 *D* shows data in cell-free and cell-embedded gels done at different distances between the iontophoresis micropipette tip and the microfiberoptic tip. Though signal amplitudes were reduced at greater separations, as expected, computed α was independent of distance between iontophoresis and microfiberoptic detection sites (Fig. 3 *D*, *inset*). Measurements of α could not be done for greater separation distances because [calcein] was reduced to <3 mM at the detection site.

These results provide experimental validation of α and D determination using the PIMP method. In the Appendix, calcein and SR fluorescence curves are computed theoretically for specified α and D, using experimentally relevant conditions. The diffusion equation was solved in three-dimensions (with spherical symmetry) subject to initial post-iontophoresis conditions and using data in Fig. 2 *C* to relate concentrations to fluorescence. Fig. 3 *E* shows computed calcein and SR fluorescence as a function of α and D. As found experimentally, the amplitudes of calcein but not SR fluorescence curves are reduced with lower α. Reduced D slows the SR fluorescence decay, but does not change the amplitudes of the calcein or SR fluorescence curves. Quantitative theoretical validation of α and D determination using Eqs. 1 and 2 is provided in Appendix.

Determination of α in solid organs in vivo

The PIMP method was applied to measure α and D in solid organs in anesthetized mice, including brain cortex, where information on the ECS exists, and kidney and skeletal muscle, where little information about α is available. Fig. 4 *A* shows the experimental set-up in which the infusion micropipette and microfiberoptic were stereotaxically inserted into brain cortex to a depth of 400 μm. Fig. 4 *B* shows the time course of calcein and SR fluorescence in brain cortex, compared with the $\alpha = 1$ reference. The reduced amplitude of calcein fluorescence in brain versus reference gel indicates that α in brain is substantially <1, whereas the kinetics of SR fluorescence decay indicates that diffusion is slowed compared with water. Data from multiple measurements in the brain gave α of 0.20 ± 0.01 and D_o/D of 3.6 ± 0.3 (Fig. 4 *D*).

We applied the PIMP method to measure α and D in two solid organs: kidney and skeletal muscle (Fig. 4 *C*). In both organs the amplitude of the calcein fluorescence signal was remarkably reduced compared to that in the $\alpha = 1$ gel or brain, yielding low α of 0.13 ± 0.02 in kidney and 0.074 ± 0.01 in skeletal muscle, with greatly decreased D (Fig. 4 *D*).

DISCUSSION

The PIMP method introduced here for measurement of extracellular space volume shares with the TMA^+ iontophoresis method the basic experimental paradigm of measuring a signal created by introduction of a probe molecule at a site near but distinct from a measurement site. However, the methods differ fundamentally in concept, as well as in execution, analysis and limitations.

The TMA^+ method involves fabrication of an elaborate triple barrel microelectrode and relies on electrophysiological detection of TMA^+ concentration using an ion-sensitive microelectrode whose tip is positioned into and thus probes the ECS at the location of the tip. The diameter of the TMA^+-sensitive microelectrode is 5–7 μm, substantially greater than ECS dimensions with typical cell-cell gaps of 50–100 nm (16). A potential concern in the TMA^+ method is whether the microelectrode tip faithfully reports TMA^+ concentration in the ECS, as probe size is much greater than ECS dimensions, and brain structure is disrupted precisely at the measurement site. Further, an ideal probe of the ECS should not interact with ECS components or brain cell membranes. It has been assumed, without direct validation, that TMA^+ is noninteractive, which may not be the case because of its size and charge. Complicating the method is significant transport of TMA^+ into brain cells during measurements, which necessitates inclusion of an independently floated permeability parameter. Because TMA^+ iontophoresis is generally done over 30 s, after which TMA^+ concentration is measured for an additional 30 s or more, the three parameters describing TMA^+ kinetics (ECS volume fraction, TMA^+ diffusion and TMA^+ permeability) are tightly coupled, requiring a complex deconvolution procedure to deduce ECS volume fraction.

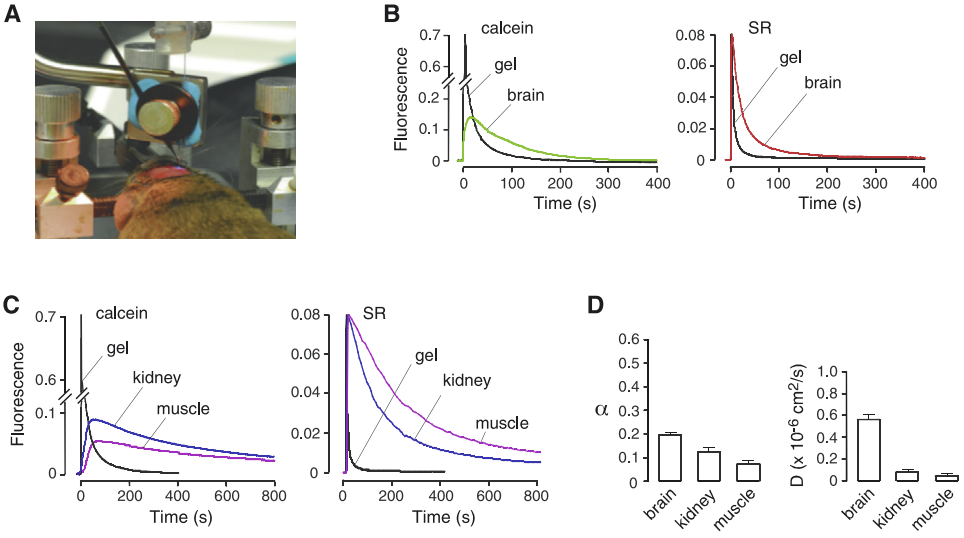

FIGURE 4 Measurement of α in solid organs in mice. (*A*) Photograph showing the dual-lumen micropipette inserted through a burr hole into the brain of a mouse whose head is immobilized on a stereotactic frame. (*B*) Calcein and SR fluorescence measured at a depth of 400 μm in brain cortex. (*C*) Time course of calcein and SR fluorescence at a depth of 400 μm in kidney and skeletal muscle. (*D*) Summary of α and D in the indicated tissues (SE, n = 3–6).

The PIMP method largely overcomes the technical concerns of the TMA^+ iontophoresis method and is simple technically and conceptually. The PIMP method requires the use of an infusion micropipette immobilized near a microfiberoptic introducing pipette. The fluorescent probes used for the PIMP measurements here, calcein and sulforhodamine 101 (SR), are established extracellular markers that are not transported into cells during the brief time of the measurement. A notable difference between the TMA^+ iontophoresis and PIMP methods is microfiberoptic detection of integrated fluorescence signal in the PIMP method, with the detected signal coming from volume elements away from, rather than directly at, the detector. Because integrated fluorescence from cell and ECS regions is measured, the PIMP method does not require introduction of a micron-sized measurement probe into the nanometer-size ECS. Another fundamental difference between the TMA^+ iontophoresis and PIMP methods is the use of an internal reference fluorescent dye in the PIMP method, assuring technical adequacy of each measurement. Another advantage of the PIMP method is that excellent fluorescence signals, with signal/noise ratio >100, are obtained after iontophoresis over 1 s or less because of the intrinsic sensitivity of fluorescence measurements and the ability to use millimolar concentrations of fluorescent dyes in the iontophoresis micropipette. The brief iontophoresis time obviates the need for multiparameter deconvolution as required to analyze TMA^+ measurements, where significant TMA^+ diffusion and cell partitioning occurs during the 30-s TMA^+ iontophoresis. Also, in contrast to the TMA^+ method, extracellular space volume determination in the PIMP method is insensitive to exact probe concentration, infusion-detection site distance, and anisotropic diffusion.

The PIMP method was validated experimentally using cell-embedded gels consisting of SP 2/0 cells suspended in 0.3% agarose gels containing specified amounts of Ficoll-70, such that ECS α and viscosity could be independently specified. Similar cell-embedded gels have been used in different types of biological applications, including studies of eosinophil activation in infection and allergy (17), cancer cell invasiveness (18), and tissue engineering (19). The excellent agreement between predicted and measured α in the cell-embedded gels provided experimental validation of the PIMP method. Measurements in which ECS viscosity was varied by addition of Ficoll-70, without changing α, validated the independent determination of α and D.

The PIMP method was applied to determine α and solute diffusion in several solid tissues in vivo. In brain cortex, α was determined to be 0.20 ± 0.01, which is in the range of reported α of 0.17–0.23 using the TMA^+ method (20–22). The (3.6 ± 0.3)-fold slowing of SR diffusion in brain cortex compared to solution deduced from the PIMP data is in agreement with D_o/D of 3.3 measured by cortical surface photobleaching (15) and 3.8 by microfiberoptic epifluorescence photobleaching (13).

The PIMP method indicated low α values of 0.13 and 0.074 and in kidney and skeletal muscle, respectively. Previous estimates of α in these organs by various methods, such as dye washout kinetics after equilibrium using ECS markers, gave α ranging from 0.25–0.6 in kidney (23,24) and 0.08–0.33 in skeletal muscle (25,26). The accuracy of these values from the older literature is questionable because of unjustified assumptions about dye penetration, interactions and cellular partitioning. More recently, in vivo magnetic resonance imaging in small animals has indicated that α is <0.1 in skeletal muscle (27), in agreement with the PIMP data.

In conclusion, the PIMP method provides a validated, technically straightforward alternative to the TMA^+ method for measurement of α and diffusion in the ECS. Using pressure-driven dye infusion in place of iontophoretic dye infusion, the method is readily extendable to measure the convection and diffusion of a wide variety of fluorescent probes of different sizes, polarities, and interactions with ECS components.

APPENDIX

We present the mathematical theory and numerical solution for fluorescent dye diffusion after iontophoresis. The goal is to compute the dependence of probe concentration, $C(r,t)$, on radial distance and time after iontophoresis, from which calcein and SR fluorescence are deduced. C(r,t) is described by Fick's Second Law,

$$\frac{\partial C}{\partial t} = D\nabla^2 C + \frac{\partial S}{\partial t}. \tag{A1}$$

D is the diffusion coefficient and S is the concentration of probe introduced by iontophoresis. Solutions to Eq. A1 for a variety of initial and boundary conditions can be found in standard references (28,29).

Strict application of Eq. A1 to the complex geometry of the extracellular space is not possible. Usually, one defines an averaging volume, V_{av}, that is large enough so that Eq. A1 is valid (12,30). The fraction of this volume that is ECS is then defined as: $\alpha = V_{ECS}/V_{av}$. The concentration of probe in Eq. A1 is the amount of probe in V_{av}. One also defines an effective diffusion coefficient, D^*, which describes translational diffusion throughout the macroscopic sample. In the physiology literature, a tortuosity parameter λ is defined, $\lambda \equiv \sqrt{D/D^*}$, where D is the diffusion coefficient in bulk ECS fluid with no obstacles to diffusion (i.e. the diffusion coefficient in water). For $\alpha < 1$, $D^* < D$ because of the tortuous path the probe must take to travel an equivalent distance compared to bulk fluid.

Experimentally, iontophoresis is carried out for a brief time with constant current, so that the amount of probe delivered is constant and independent of α. As α decreases at constant iontophoresis time, the number of probe molecules within an observation volume, V_{fo}, remains constant. However, probe concentration in V_{ECS} increases because of reduced V_{ECS} with decreasing α. This assumes that the probe is confined to the ECS and does not diffuse into the cells. SR and calcein are good extracellular markers that do not diffuse significantly into cells over the time course of the experiments.

We assume that the characteristic times for iontophoresis (1 s) and diffusion (10–70 s) are well enough separated so that iontophoresis occurs without significant diffusion. We also assume that the system is spherically symmetric, so that Eq. A1 reduces to (28)

$$\frac{\partial C}{\partial t} = D\left(\frac{\partial^2 C^*}{\partial r^2} + \frac{2}{r}\frac{\partial C^*}{\partial r}\right). \tag{A2}$$

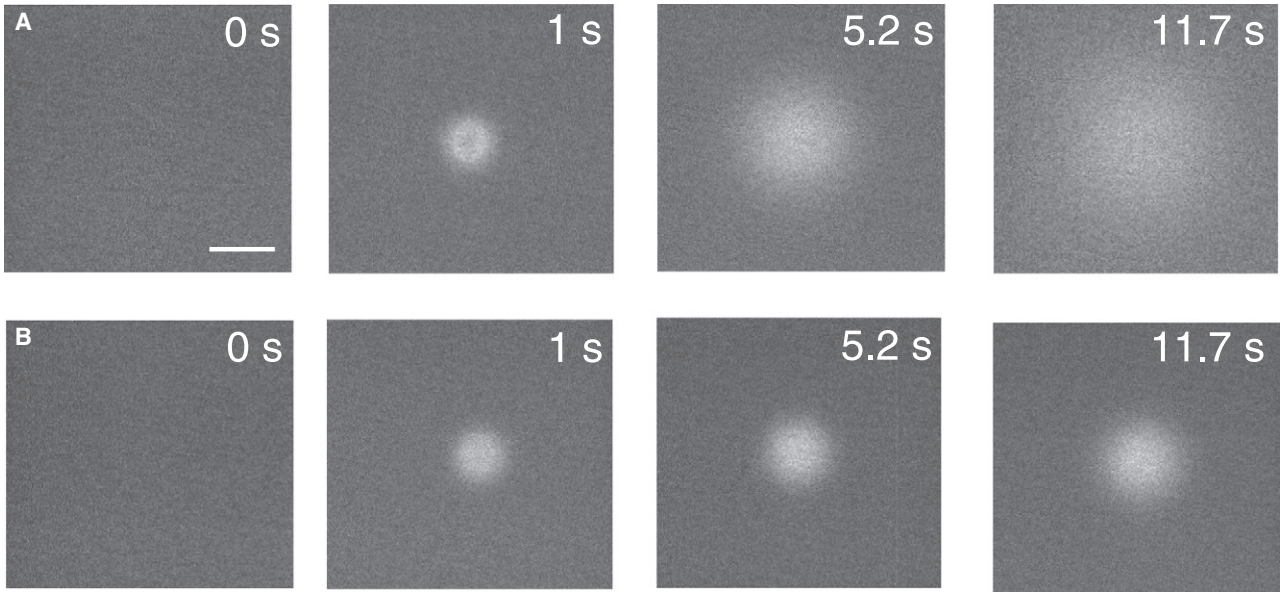

FIGURE 5 Imaging of SR iontophoresis and diffusion. (*A*) SR fluorescence images in a 0.3% agarose gel at indicated times after start of iontophoresis. Iontophoresis was done at constant current for 1 s. Bar, 100 μm. (*B*) SR fluorescence images in a 0.3% agarose gel containing cells ($\alpha = 0.16$). Though profiles just after iontophoresis are similar, the spread of SR fluorescence is much slower in the presence of cells because of tortuous path the probe must take to move around the cells.

Equation A2 can be transformed to the one-dimensional diffusion equation with the substitution $u = rC^*$,

$$\frac{\partial u}{\partial t} = D\frac{\partial^2 u}{\partial r^2}. \tag{A3}$$

The initial concentration profile after iontophoresis was estimated by imaging, in thin agarose gels, the spread of SR fluorescence from the iontophoresis tip in the absence of the fiberoptic (Fig. 5) After iontophoresis the dye is transported well beyond the 20 μm separation of the iontophoresis micropipette and fiberoptic detector. In most simulations, we assume from image analysis that the initial concentration profile is a Gaussian function with half-width at half-height of 35 μm. Different initial concentration profiles (combinations of square, trapezoidal, and exponential functions) did not significantly alter α or D as computed using Eqs. 1 and 2 in the text.

Equation A3 was solved for a specified initial concentration profile and appropriate boundary conditions ($u = 0$ at $r = 0$ and $r = \infty$) using the iterative Crank-Nicolson method (31). The parameter $D\Delta t/(\Delta x)^2$ was held fixed at 0.0325, where Δt and Δx are the grid parameters for time and space, respectively. $D\Delta t/(\Delta x)^2$ was determined empirically such that further reductions in the grid parameters did not affect computed concentration profiles. Concentrations were recovered from u by $C^* = u/r$ after numerical solution of Eq. A3.

To relate the experimentally measured fluorescence intensities, F, to C*, calibration measurements were done (Fig. 2 *C* in main text). Note that the probe concentration used in the calibration plots corresponds to C, the concentration of probe in V_{ECS}, not C^*, the concentration of probe in V_{fo}. The two concentrations are related by $C^* = \alpha C$.

Fluorescence profiles of F_{SR} and F_{cal} were computed at different times after iontophoresis (Fig. 6 *A*). For SR, the fluorescence intensity decays as expected for dissipation of a concentration gradient in one dimension. For calcein, however, the fluorescence decay is biphasic because the dissipation of the concentration gradient is convolved with self-quenching. Calcein self-quenching is thought to be due to a combination of dimerization, energy transfer to nonfluorescent dimers, and collisional quenching between dye monomers (32). At short times after iontophoresis, calcein fluorescence is quenched near the iontophoresis tip. At longer times after iontophoresis, calcein concentration decreases near the iontophoresis tip, but the fluorescence increases because of reduced calcein self-quenching. Once the fluorescence reaches the maximum corresponding to [calcein] $\approx$ 3 mM, further

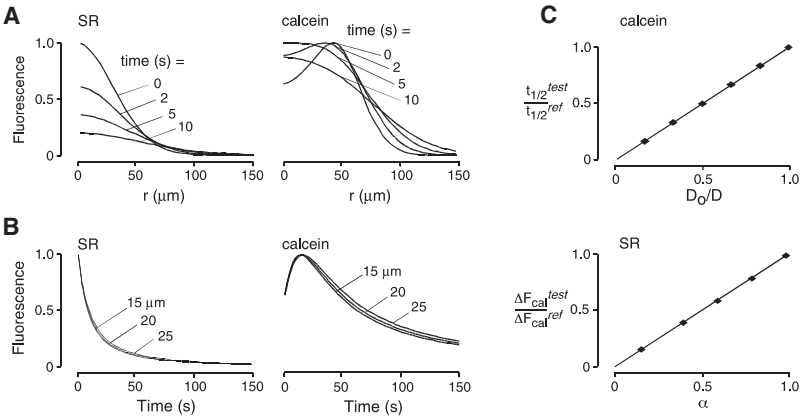

FIGURE 6 Simulation of SR and calcein fluorescence. (*A*) Fluorescence intensity profiles of SR (*left*) and calcein (*right*). Data computed over 800 μm with a time step of 50 μs, distance step of 0.392 μm, $\alpha = 1$, and $D = 100\ \mu m^2/s$. (*B*) Effect of distance between iontophoresis tip and fiberoptic probe on the SR (*left*) and calcein (*right*) time courses. Data were simulated as in (*B*) for tip-probe distances of 15, 20, and 25 μm. (*C*) Validation of α and D determination from calcein and SR fluorescence time course. Calcein (*top*) and SR (*bottom*) fluorescence time courses were simulated for $D = 100\ \mu m^2/s$ and specified α. Ratios of fluorescence amplitudes and half-times, calculated by Eqs. 1 and 2 of the text, respectively, are given on the ordinate. The solid line is the line of identity.

reductions in calcein concentrations near the iontophoresis tip result in decreased fluorescence. In effect, the fluorescence at a point near the iontophoresis tip follows the self-quenching curve as calcein concentration decreases. The consequence is a biphasic change in calcein fluorescence after iontophoresis. The biphasic response is observed only when initial calcein concentration is >~3 mM, the peak in the self-quenching curve.

Simulated fluorescence time courses of F_{SR} at different r are given in Fig. 6 *B*. Variation of $\pm$ 5 μm between the iontophoresis tip and the fiberoptic had little effect on the time course. Typical values of the tortuosity parameter, λ, estimated from the half-time of SR fluorescence decay as described in the text, varied by $\pm$ 9%. Importantly, determination of α is strictly independent of the distance between the fiberoptic detector and the iontophoresis tip, such that the precise placement of the fiberoptic relative to the iontophoresis tip is not critical, provided that iontophoresis is sufficient to increase calcein concentration above ~3 mM at the detection site.

Last, simulations were done to formally validate the Eqs. 1 and 2 in the text and to compute α and D. To validate determination of α, calcein fluorescence time courses were simulated at constant D and varying α. The maximum fluorescence amplitude was then determined from the simulated data. Fig. 6 *C* (*top*) shows that values of α are indeed proportional to $\Delta F_{cal}^{test}/\Delta F_{cal}^{ref}$ (where ref refers to $\alpha = 1$ reference gel sample), as predicted by Eq. 1 of the text. To validate determination of D, SR fluorescence time courses were simulated at constant $\alpha = 1$ and varying D (50−300 $\mu m^2/s$). Half-times for fluorescence decay were determined from the simulated data. Fig. 6 *C* (*bottom*) shows that the relative diffusion coefficient of SR is proportional to $t_{1/2}^{ref}/t_{1/2}^{test}$, as predicted by Eq. 2 of the text.

We thank Dr. Marios Papadopoulos for technical help and advice on brain ECS measurements, and Drs. Songwan Jin and Zsolt Zador for help in the early phase of the project.

This work was supported by grants EB00415, DK35124, EY13574, HL59198, DK72517, and HL73856 from the National Institutes of Health, and Research Development Program and Drug Discovery grants from the Cystic Fibrosis Foundation.

REFERENCES

1. Nicholson, C., K. C. Chen, S. Hrabetova, and L. Tao. 2000. Diffusion of molecules in brain extracellular space: theory and experiment. *Prog. Brain Res.* 125:129–154.
2. Sykova, E. 2004. Diffusion properties of the brain in health and disease. *Neurochem. Int.* 45:453–466.
3. Somjen, G. G. 2002. Ion regulation in the brain: implications for pathophysiology. *Neuroscientist.* 8:254–267.
4. Sykova, E., and L. Vargova. 2008. Extrasynaptic transmission and the diffusion parameters of the extracellular space. *Neurochem. Int.* 52:5–13.
5. Law, R. O. 1982. Techniques and applications of extracellular space determination in mammalian tissues. *Experientia.* 4:411–421.
6. Krol, A., J. Maresca, M. W. Dewhirst, and F. Yuan. 1999. Available volume fraction of macromolecules in the extravascular space of a fibrosarcoma: implications for drug delivery. *Cancer Res.* 59:4136–4141.
7. Nagano, S., J. Y. Perentes, R. K. Jain, and Y. Boucher. 2008. Cancer cell death enhances the penetration and efficacy of oncolytic herpes simplex virus in tumors. *Cancer Res.* 68:3795–3802.
8. Stroh, M., W. R. Zipfel, R. M. Williams, W. W. Webb, and W. M. Saltzman. 2003. Diffusion of nerve growth factor in rat striatum as determined by multiphoton microscopy. *Biophys. J.* 85:581–588.
9. Alexandrakis, G., E. B. Brown, R. T. Tong, T. D. McKee, R. B. Campbell, et al. 2004. Two-photon fluorescence correlation microscopy reveals the two-phase nature of transport in tumors. *Nat. Med.* 10:203–207.
10. Thiagarajah, J. R., J. K. Kim, M. Magzoub, and A. S. Verkman. 2006. Slowed diffusion in tumors revealed by microfiberoptic epifluorescence photobleaching. *Nat. Methods.* 3:275–280.
11. Zheng, K., A. Scimemi, and D. A. Rusakov. 2008. Receptor actions of synaptically released glutamate: the role of transporters on the scale from nanometers to microns. *Biophys. J.* 95:4584–4596.
12. Nicholson, C., and J. M. Phillips. 1981. Ion diffusion modified by tortuosity and volume fraction in the extracellular microenvironment of the rat cerebellum. *J. Physiol.* 321:225–257.
13. Zador, Z., M. Magzoub, S. Jin, G. T. Manley, M. C. Papadopoulos, et al. 2008. Microfiberoptic fluorescence photobleaching reveals size-dependent macromolecule diffusion in extracellular space deep in brain. *FASEB J.* 22:870–879.
14. Dauty, E., and A. S. Verkman. 2004. Molecular crowding reduces to a similar extent the diffusion of small solutes and macromolecules: measurement by fluorescence correlation spectroscopy. *J. Mol. Recognit.* 17:441–447.
15. Binder, D. K., M. C. Papadopoulos, P. M. Haggie, and A. S. Verkman. 2004. In vivo measurement of brain extracellular space diffusion by cortical surface photobleaching. *J. Neurosci.* 24:8049–8056.
16. van Harreveld, A., and S. K. Malhotra. 1967. Extracellular space in the cerebral cortex of the mouse. *J. Anat.* 101:197–207.
17. Tedla, N., C. Bandeira-Melo, P. Tassinari, D. E. Sloane, M. Samplaski, et al. 2003. Activation of human eosinophils through leukocyte immunoglobulin-like receptor 7. *Proc. Natl. Acad. Sci. USA.* 100:1174–1179.
18. Che, Z. M., T. H. Jung, J. H. Choi, J. Yoon, H. J. Jeong, et al. 2006. Collagen-based co-culture for invasive study on cancer cells-fibroblasts interaction. *Biochem. Biophys. Res. Commun.* 346:268–275.
19. Wu, M. H., J. P. Urban, Z. F. Cui, Z. Cui, and X. Xu. 2007. Effect of extracellular ph on matrix synthesis by chondrocytes in 3D agarose gel. *Biotechnol. Prog.* 23:430–434.
20. Sykova, E., I. Vorisek, T. Mazel, T. Antonova, and M. Schachner. 2005. Reduced extracellular space in the brain of tenascin-R- and HNK-1-sulphotransferase deficient mice. *Eur. J. Neurosci.* 22:1873–1880.
21. Sykova, E., I. Vorisek, T. Antonova, T. Mazel, M. Meyer-Luehmann, et al. 2005. Changes in extracellular space size and geometry in APP23 transgenic mice: a model of Alzheimer's disease. *Proc. Natl. Acad. Sci. USA.* 102:479–484.
22. Anderova, M., S. Kubinova, T. Mazel, A. Chvatal, C. Eliasson, et al. 2001. Effect of elevated K^+, hypotonic stress, and cortical spreading depression on astrocyte swelling in GFAP-deficient mice. *Glia.* 35:189–203.
23. Maxild, J., J. V. Moller, and M. I. Sheikh. 1981. An energy-dependent, sodium-independent component of active p-aminohippurate transport in rabbit renal cortex. *J. Physiol.* 310:273–283.
24. Rosenberg, L. E., S. J. Downing, and S. Segal. 1962. Extracellular space estimation in rat kidney slices using C saccharides and phlorizin. *Am. J. Physiol.* 202:800–804.
25. Poole-Wilson, P. A., and I. R. Cameron. 1975. ECS, intracellular pH, and electrolytes of cardiac and skeletal muscle. *Am. J. Physiol.* 229:1299–1304.
26. Cooper, J. G., and P. G. Kohn. 1980. Alpha-aminoisobutyric acid transport in rat soleus muscle and its modification by membrane stabilizers and insulin. *J. Physiol.* 302:89–105.
27. Vincensini, D., V. Dedieu, J. P. Renou, P. Otal, and F. Joffre. 2003. Measurements of extracellular volume fraction and capillary permeability in tissues using dynamic spin-lattice relaxometry: studies in rabbit muscles. *Magn. Reson. Imaging.* 21:85–93.
28. Crank, J. 1975. The Mathematics of Diffusion. Oxford University Press, Oxford.
29. Carslaw, H. S., and J. C. Jaeger. 1959. Conduction of Heat in Solids. Clarendon Press, Oxford.
30. Lehner, F. K. 1979. Validity of Fick's Law for transient diffusion through a porous medium. *Chem. Eng. Sci.* 34:821–825.
31. Crank, J., and P. Nicolson. 1947. A practical method for numerical evaluation of solutions of partial differential equations of the heat conduction type. *Proc. Camb. Philol. Soc.* 43:50–64.
32. Chen, R. F., and J. R. Knutson. 1988. Mechanism of fluorescence concentration quenching of carboxyfluorescein in liposomes: energy transfer to nonfluorescent dimers. *Anal. Biochem.* 172:61–77.